International Journal of Green Energy

ISSN: 1543-5075 (Print) 1543-5083 (Online) Journal homepage: https://www.tandfonline.com/loi/ljge20

Improving photostability and efficiency of polymeric luminescent solar concentrators by PMMA/MgO nanohybrid coatings

S. M. El-Bashir, I.S. Yahia, F. Al-Harbi, H. Elburaih, F. Al-Faifi & N. A. Aldosari

To cite this article: S. M. El-Bashir, I.S. Yahia, F. Al-Harbi, H. Elburaih, F. Al-Faifi & N. A. Aldosari (2017) Improving photostability and efficiency of polymeric luminescent solar concentrators by PMMA/MgO nanohybrid coatings, International Journal of Green Energy, 14:3, 270-278, DOI: 10.1080/15435075.2016.1233422

To link to this article: https://doi.org/10.1080/15435075.2016.1233422

Published online: 26 Jan 2017.

INTERNATIONAL JOURNAL OF GREEN ENERGY
2017, VOL. 14, NO. 3, 270–278
http://dx.doi.org/10.1080/15435075.2016.1233422

Taylor & Francis
Taylor & Francis Group

Improving photostability and efficiency of polymeric luminescent solar concentrators by PMMA/MgO nanohybrid coatings

S. M. El-Bashir[a,b], I.S. Yahia[c,d], F. Al-Harbi[e], H. Elburaih[e], F. Al-Faifi[a], and N. A. Aldosari[f]

[a]Department of Physics & Astronomy, Science College, King Saud University, Riyadh, Saudi Arabia; [b]Department of Physics, Faculty of Science, Benha University, Benha, Egypt; [c]Department of Physics, Faculty of Science, King Khalid University, Abha, Saudi Arabia; [d]Physics Department, Nano-Science & Semiconductor Labs, Faculty of Education, Ain Shams University, Roxy, Cairo, Egypt; [e]Department of Physics, College of Science, Princess Nora Bint Abdulrahman University, Riyadh, Saudi Arabia; [f]Physics Department, College of Sciences and Humanities, Salman Bin Abdulaziz University, Alkharj, Saudi Arabia

ABSTRACT

MgO nanocrystals were synthesized and doped with different concentrations in poly(methylmethacrylate) (PMMA) to prepare hybrid organic-inorganic coatings based on polymer nanohybrid thin films. The nanoparticles were found to be spherical with 62 nm diameter as determined by X-ray diffraction (XRD) and atomic force microscope (AFM). The coatings were characterized by spectroscopic tools such as optical absorption, transmission and fluorescence spectroscopy. The prepared nanohybrid films were spin-coated on cost-effective luminescent PMMA substrates doped with highly efficient luminescent dyes luminescent solar concentrators (LSCs). The outdoor photostability tests demonstrated enhanced protection against UVA radiation for coated LSCs compared to bare LSC substrates. The current–voltage characteristics of commercially produced LSC prototypes showed that the poor UV response of monocrystalline silicon solar cell can be improved by for LSCs coated by PMMA/MgO nanohybrid films which act as luminescent down shifting layer (LDSL).

ARTICLE HISTORY
Received 10 May 2015
Accepted 3 September 2016

KEYWORDS
Luminescent solar concentrator; photoluminescence; photostability; PMMA nanohybrids; textured monocrystalline silicon PV cell

Introduction

The importance of solar energy is growing as a clean and renewable energy source, as many of the conventional sources are being increasingly diminishing. Many different kinds of photovoltaic (PV) cells have been developed, there are multiple categories of PV cells according to material, efficiency, cost and applications. The high cost of PV cells made from monocrystalline silicon (c-Si) and the diffuse nature of sunlight have ensured that silicon PV cells cannot be generally applied for economic large-scale electric power generation. Luminescent solar concentrators (LSCs) have been proposed since the late 1970s as a promising approaches for lowering the cost of PV panels by replacing the large area of expensive PV cells with an inexpensive polymeric concentrator, thereby reducing the cost of the module (in dollars per watt) and also of the solar power (in dollars per kilowatt/hour) (Rowan, Wilson, and Richards 2008). The idea of LSCs is based on a waveguide in which the luminescent materials are dispersed into a transparent substrate with a high refractive index. Solar light can be absorbed and re-emitted by the luminescent materials. Most of the fluorescent photons are trapped in the waveguide by total internal reflection and transported to the side edges where PV cells are attached (Debije and Verbunt 2012). Compared to traditional geometrical concentrators, LSCs can collect both direct and diffuse sunlight without depending on the configuration, meaning that solar photons can be concentrated in cloudy weather and at any time of the day (El-Bashir 2013b). Many papers had been reported on thin-film LSC devices which consist of a thin layer of a luminescent film casted onto a clear substrate for better optical efficiency (Dienel et al. 2010; Wiegman and Van Der Kolk 2012) or a high refractive index film coated on a luminescent substrate for enhanced stability specially in hot countries (El-Bashir 2014b; El-Bashir 2013a; Goldschmidt et al. 2009). Recently, efforts have been made to increase the power conversion efficiency of LSCs in different ways including using of spectrally matched solar cells (Goldschmidt et al. 2009)and searching new materials such as surface plasmons, quantum dots, flexible matrices, photonic layers and liquid crystals (Griffini, Levi, and Turri 2014, Griffini, Levi, and Turri 2013; Carlotti et al. 2016).

This paper represents a novel type of thin-film LSCs which consists of commercial luminescent polymethylmethacrylate (PMMA) plates coated with PMMA/MgO nanohybrid films prepared in our laboratories. We selected MgO NCs as they have a promising UV-shielding capability as they reduce the damage effect of different kinds of UV radiation (Dadvar, Tavanai, and Morshed 2011; Zhang et al. 2012) which is abundant on the earth´s atmosphere and causes the yellowness of the polymeric matrix. Additionally, the proposed PMMA/MgO nanohybrid films can act as a luminescent downshifting layer (LDSL) which can convert high energy photons (UV and blue) of solar spectra, that are inefficiently used by c-Si PV cell, to visible photons that can be located in the area of PV cell

CONTACT S. M. El-Bashir elbashireg@yahoo.com Department of Physics, Faculty of Science, Benha University, Benha, Egypt.
Color versions of one or more of the figures in the article can be found online at www.tandfonline.com/ljge.

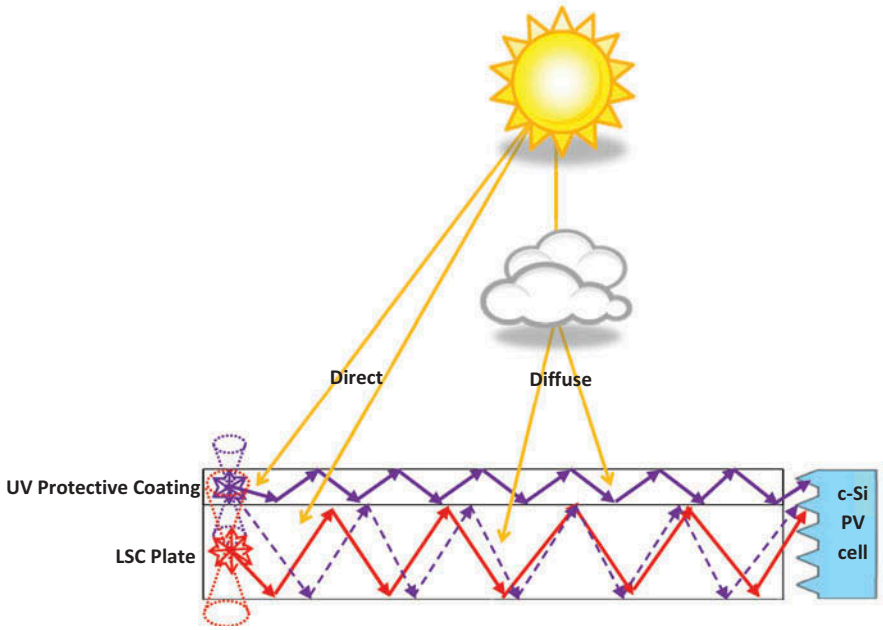

Figure 1. A Schematic diagram of LSC coated by UV protective nanocomposite film.

sensitivity. The performance of thin-film LSC prototypes will be evaluated using a low-cost simple optical design showed in Figure 1, which implies concentrating sunlight on textured c-Si PV cells that are locally manufactured. The usage of textured c-Si PV cells has several advantages such as reducing of the reflective losses by redirecting the luminescent photons to be trapped into the surface of c-Si PV cell (Yahia, Yakuphanoglu, and Azim 2011; Edwards et al. 2008).

Experimental

Preparation of PMMA/MgO nanohybrid films

Magnesium oxide nanocrystals (MgO NCs) were prepared by co-precipitation method as follows, 2 M of $MgCl_2$ $2H_2O$ precursor was prepared by dissolving 190.422 g $MgCl_2$ (Aldrich, USA) in 1 L water. Then the precursor was dissolved along with NaOH in deionized water in separately beakers at 50°C for 1 hr to have transparent and clear solutions. After complete dissolving of $MgCl_2$ $2H_2O$; NaOH solution was added drop by drop until the clear solution inched to a white precipitate and the colloidal solution was stirred for another hour to complete the reaction. The precipitate was collected by filtration and washed with deionized water several times and then by ethanol as a last stage. After washing, the final product was dried at 150°C for 2 hr, then the dried powder was inserted in high temperature furnace for calcination at 500°C for 3 hr to remove any organic residuals inside the nanopowder. PMMA pellets obtained from (SABIC, KSA) were dissolved in Dichloromethane (CH_2Cl_2) (Aldrich, USA) with concentration 7 g/100 mL to obtain PMMA solution. In order to obtain good quality of the casted films, MgO NCs were dispersed throughout the polymer solution with different concentrations (5, 10 and 20 wt%) and sonicated for 3 hr at 40°C. Subsequently the solutions were cast onto glass dishes and then left to be dry. After drying, the films were removed and heated at 50◦C for 4 hr to attain a complete evaporation of the confined solvent molecules. All the film thicknesses were determined using the Fizau fringe technique (El-Bashir 2012) and were found to be of the order of 50 ± 5 μm.

Preparation of LSC prototypes

Three millimeters thick luminescent PMMA sheets (FOSG1®, FOSY1® and FOSR1®) were obtained from (SPIROPLAST Co., Egypt). As observed by naked eye in Figure 2(a), the plates have a wide range of visible wavelengths and strongly shining even underindoor illuminations. The sheets were cut into six LSC plates with dimensions of 20 cm × 8 cm × 0.3 cm, two groups LSC prototypes were manufactured for Laboratory *I–V* testing as shown in Figure 3. The first group consists of the uncoated original PMMA luminescent plates and the second was prepared from UV protected PMMA luminescent plates which are coated by PMMA/MgO nanohybrid films using a home-made spin coating technique at 1000 rpm (Hammam et al. 2007) for 60 sec. The prepared LSC prototypes were attached to c-Si PV cells (Arab Int. Optronics Co., Egypt) and the *I–V* characteristics was performed as illustrated by Figure 3 under 100 mW/cm^2 illumination using a 100 W halogen light bulb calibrated in sunlight equivalents to perform all measurements indoors as described in the literature (Du Pasquier, Miller, and Chhowalla 2006).

Measurements and characterization

Fully automated Atomic force microscope (AFM) (NT-MDT SOLVER NEXT, Russia), was used for characterization of nanoporous MgO in semi-contact mode. X-ray diffraction (XRD) patterns were obtained by X-ray diffractometer (SHIMADZUXRD-6100, Japan), using *CuKα* (λ = 1.5406 Å) radiation over 2θ range from 5 to 90° with continuous scan speed was 2 deg/min. The spectral response of c-Si PV cell

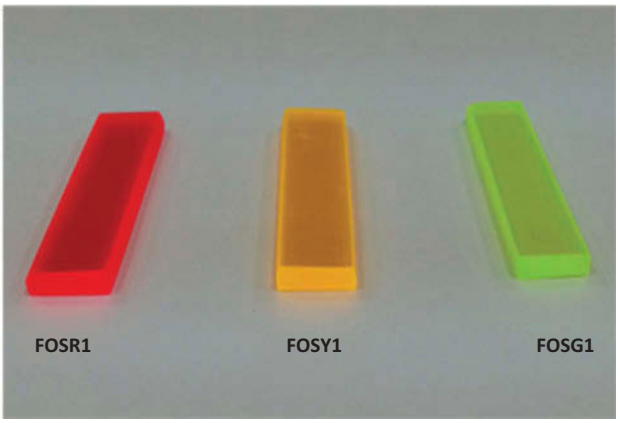

(a)

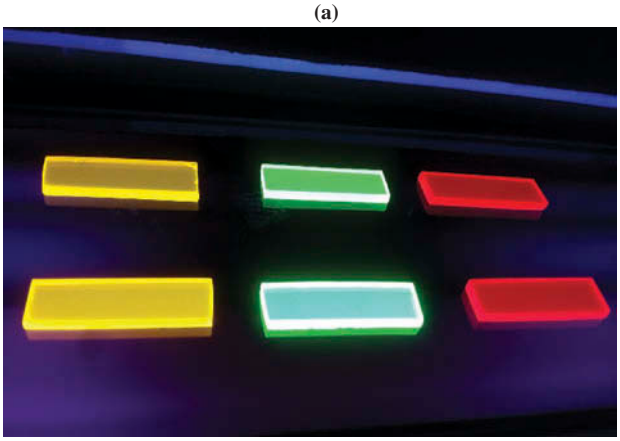

(b)

Figure 2. (a) LSC samples and (b) UV irradiation of LSC samples.

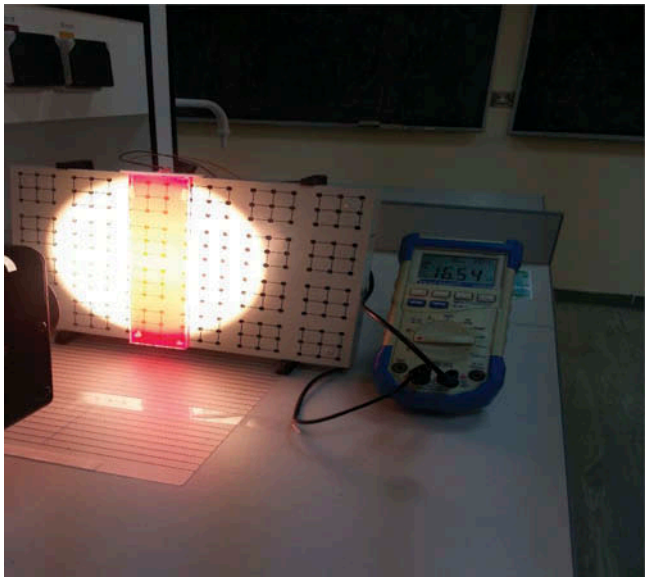

Figure 3. Laboratory *I–V* testing of coated LSC FOSR1®.

was determined using a calibrated home-built setup for external quantum efficiency (EQE) measurements, consisting of 1000 W xenon lamp, a high quality direct drive scanning monochromator (Omni-λ150, UK), four 100 W halogen lamps for bias illumination, a motorized six position filter wheel (MSZ3122, Germany), *I–V* convertor (MellesGriot, UK), DSP Lock-In Amplifier (SR830, Stanford Inc., USA) and optical chopper system with chopping frequencies from 1 Hz to 10 kHz (THORLABS: MC2000, USA). The absorption spectra were recorded in the wavelength range (190–900 nm) using a UV-VIS spectrophotometer (UNICAM, Helios Co., Germany). Specular reflectance was measured using a double-beam spectrophotometer (SHIMADZU UV-3101PC, Japan). The steady-state fluorescence spectra were recorded in the wavelength range (200–900 nm) using a spectrofluorimeter (SHIMADZU RF-5301 PC, Japan). The fluorescence spectra were recorded at the excitation wavelengths of the absorption maxima "λ_a" of each sample listed in Table 1. Laboratory studies of the photostability for coated and uncoated LSC prototypes towards UV radiation,had been performed by subjecting (1 cm × 4 cm) samples to UV lamps (6 watts, 254/365 nm wavelength, 115 VAC/60 Hz, Cole Parmer, USA) for 96 hr as depicted by Figure 2(b). The outdoor photostability tests for coated and uncoated LSCs had been performed for 5 weeks of continuous exposure to natural sunlight at Riyadh city (August 2013-KSA). The thermal effect of high ambient temperature was eliminated by cooling LSC samples using a simple home-made water circulation system by which the temperature of LSC samples can be lowered to about 32°C.

Table 1. The absorption peak $\lambda_{a(max)}$, the corresponding band Δ_a, the fluorescence maximum $\lambda_{f(max)}$, the corresponding FWHM bands, and the fluorescence quantum yield ϕ_f of the investigated LSCs and the prepared UV protective coating.

Sample	$\lambda_{a(max)}$ (nm)	Δ_a (nm)	$\lambda_{f(max)}$ (nm)	Δ_f (nm)	ϕ_f
Coating	320	280–355	400	380–435	0.21
FOSG1	475	400–485	507	490–531	0.67
FOSY1	525	400–545	572	547–586	0.79
FOSR1	570	514–495	615	602–635	0.87

Results and discussion

Characterization & structure of MgONCs

Figure 4 presents a typical topographic 2D and 3D AFM images of the synthesized MgO NCs obtained using semi-contact mode, the images showed small individual particles along with larger agglomerates. The analysis of the grain size was done by the Image Analyzer software attached to the microscope and the mean value of the MgO NCs grain size is equal to 62 nm.

The XRD pattern for the as-prepared MgO powder is presented in Figure 5, it can be seen that MgO nanoparticles have a highly crystalline nature. The peaks of MgO were appeared at $2\theta^o$ values equal 36.868, 42.855, 62.184, 74.562 and 78.468 which are corresponding to (111), (200), (220), (311) and (222) planes according the JCDPS card No. (89–4248) (JCDPS 2002). From this study it can be confirmed that MgO is the only dominant phase and no other phases appeared, additionally the pattern revealed that pure MgO have cubic structure. The lattice constants*a*for pure MgO nanocrystals were obtained from the interplanar spacing of d_{hkl} value of the (200) and (220) peaks using the following equation (Kittel 1976):

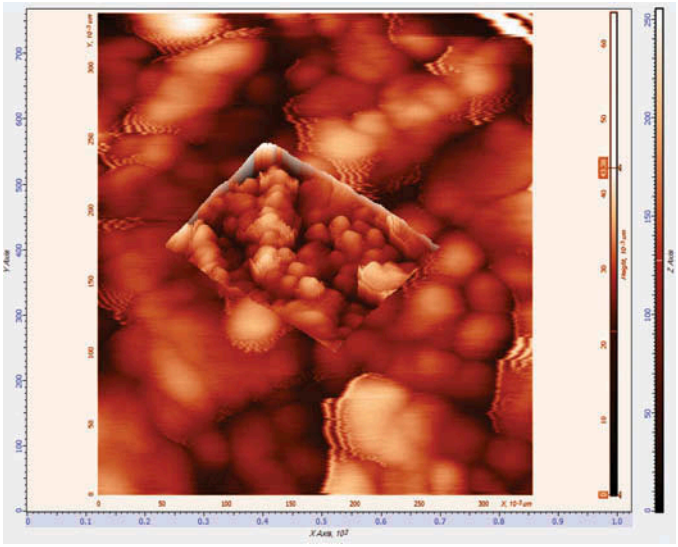

Figure 4. 2D and 3D (inset) AFM micrographs for pure of MgO NPs.

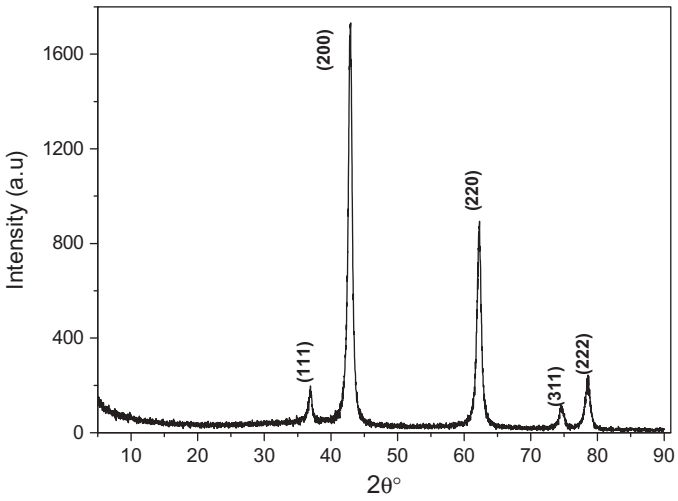

Figure 5. X-ray diffraction for pure MgO NPs.

$$d_{hkl} = \frac{a}{\sqrt{h^2 + k^2 + l^2}} \quad (1)$$

The mean value of the calculated lattice constant a for pure MgO nanocrystals was 4.218 Å, which is found to be in good agreement with reported value on JCDPS card No.89–4248 which equal 4.211 Å. The crystallite size of pure MgO nanocrystals was be calculated depending on the full width at half maximum (FWHM) and the diffraction angle θ known as Scherrer's equation (Cullity 1956):

$$D = \frac{0.9\lambda}{\beta \cos\theta} \quad (2)$$

where β is the full-width at half maximum for the recorded peaks appearing at the diffraction angle θ, the crystallite size was calculated giving the mean value of the crystallite size as 13.2 nm. Depending on the values of β, θ and D, it is possible to calculate the dislocation density δ and crystal strain ε for the studied materials as follows (Murali et al. 2010):

$$\delta = \frac{n}{D^2} \quad (3)$$

$$\varepsilon = \frac{\beta \cos\theta}{4} \quad (4)$$

where n is taken as unity at a minimum dislocation density, the presence of dislocations strongly influences many of the properties of materials (Callister 1997). The values of the dislocation density δ and crystal strain $\varepsilon$for pure MgO are 5.792×10^{-3} nm^{-2} and 2.634×10^{-3}, respectively.

Spectral properties of PMMA/MgO nanohybrids for LSC coating applications

The concentration effect of MgO NCs on the UV absorption spectra of PMMA/MgO nanohybrid films is shown in Figure 6, a broad absorption band with two maxima had been appeared at 297 and 340 nm. The red shift observed in the band edge by increasing the concentration MgO NCs can be attributed to the increase of the contributions from surface F-centers whose energies cover a broad sub-band gap range (Stankic et al. 2007). In addition, it is observed that the absorption in the UVA and UVB regions was increased to three folds by increasing MgO NCs to 20 wt%, this indicates the promising reduction of the transmitted amount of UV radiation by these films when applied as LSC coatings. This means that the UV transmittance of PMMA can be reduced by increasing the concentration of MgO NCs; pointing to that PMMA/MgO nanohybrid films are promising UV protective coatings for LSCs which can alleviate the photodegradation of luminescent dyes.

The spectral distribution of the reflectance is shown in Figure 7(a) for PMMA/MgO nanohybrid films measured at the normal light incidence in the wavelength range 300–1100 nm. It is clear from the spectral behavior of $R(\lambda)$ that the film reflectance is increased by increasing MgO NCs without altering the quality of the film homogeneity. The approximate value of the refractive index (n) can be calculated using the following formula (Roncali and Garnier 1984):

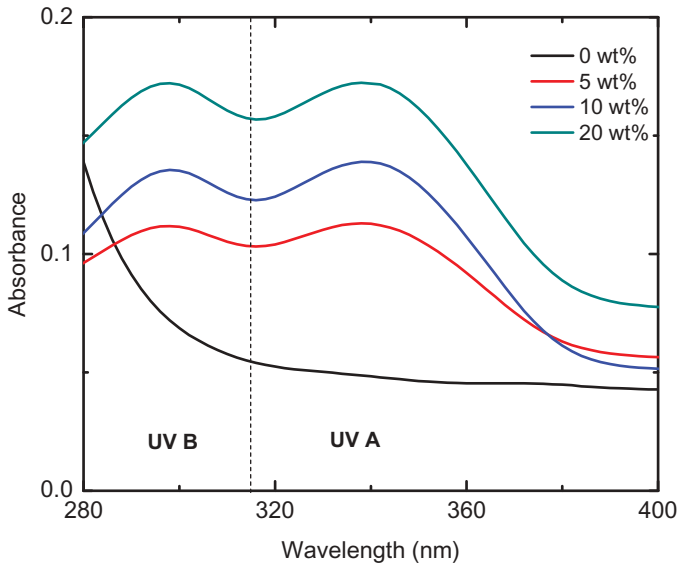

Figure 6. UV absorption spectra for PMMA/MgOnanocomposite films.

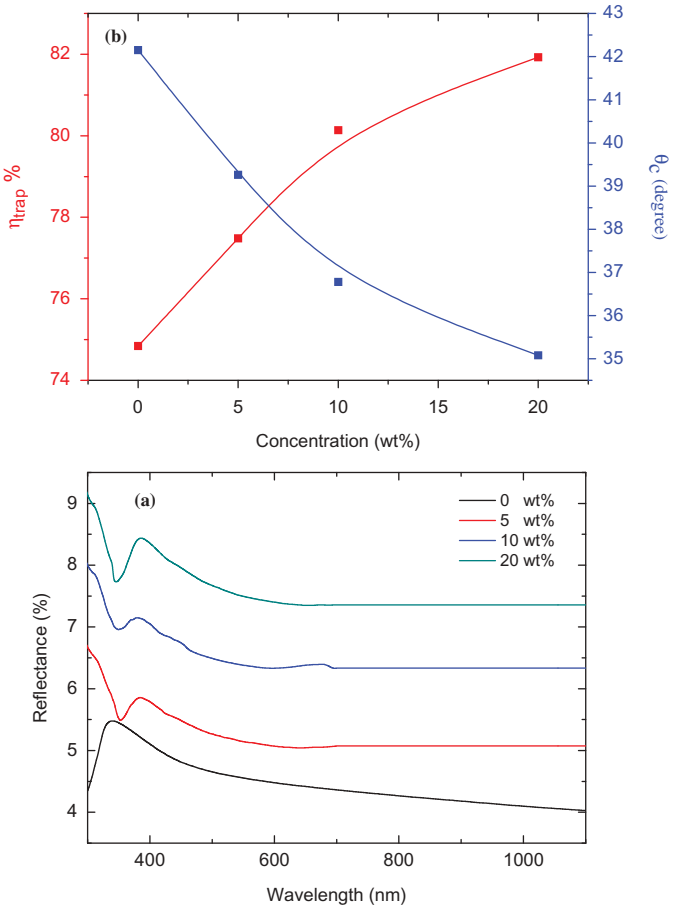

Figure 7. (a) Specular reflectance spectra and (b) the corresponding critical angle and photon trapping efficiency for PMMA/MgO nanocomposite films.

$$n = \frac{1+\sqrt{R}}{1-\sqrt{R}} \tag{5}$$

where (R) is the film reflectance recorded from the specular reflection spectra measured at normal light incidence, part of the fluorescent photons falls within the escape cone determined by the critical angle θ_c and is lost from LSC surface as illustrated in Figure 1. The critical angle is defined by:

$$\theta_c = \sin^{-1}\left(\frac{1}{n}\right) \tag{6}$$

and the trapping efficiency η_{trap}, which is defined as the fraction of luminescent photons emitted outside the escape cone, had been calculated the from the formula (Batchelder, Zewail, and Cole 1979):

$$\eta_{trap=\cos(\theta_c)} \tag{7}$$

Figure 7(b) shows the dependence of θ_c and η_{trap} on MgO NCs concentration, it is noted that all the films have a reduced critical angle loss since the value of θ_c is remarkably decreased from 42.16° for pure PMMA to a minimum value about 35.08° for PMMA film doped with 20 wt% MgO NCs. The calculated values of η_{trap} showed a significant increase from 74.84% for pure PMMA to 81.93% for PMMA film doped with 20 wt% MgO NCs. This advantage lead to the reduction of the fraction of escaped luminescent photons from the critical cones and accordingly improving solar energy conversion efficiency obtained by LSCs coated by these nanohybrid films. Besides, it is revealed that PMMA/MgO nanohybrid thin film permits the trapping of a larger fraction of luminescent photons and consequently improves the guiding properties and optical efficiency of LSCs (de Boer et al. 2012).

Figure 8 shows the absorption spectra of the investigated LSC plates, it is clear that each plate has a wide absorption band in the visible solar spectrum at AM1.5. The absorption and fluorescence peaks $\lambda_{a(max)}$ and $\lambda_{f(max)}$ for LSC samples and the prepared UV protective coating, were estimated at FWHM. Additionally, the absolute fluorescence quantum yield(ϕ_F) were calculated as mentioned in Ref. (Crosby and Demas 1971) using the following equation:

$$\phi_F = \phi_{ref}\left(a/a_{ref}\right)\left(n/n_{ref}\right)\left(S_{ref}/S\right) \tag{8}$$

where ϕ_{ref} is the fluorescence quantum yield of the standard reference which is chosen to be located in the same fluorescence region of the measured material (a) is the absorbance, n is the refractive index of the matrix and S is the area under the fluorescence curve, the values of $\lambda_{a(max)}$,$_{F(max)}$ and ϕ_F are listed in Table (1). From this spectroscopic data, it is clear all the samples have promising values of ϕ_F for better harvesting of solar radiation across the full visible spectrum.

The external quantum efficiency (EQE) of c-Si PV cell, the fluorescence spectra of LSC plates and the optimized UV fluorescent protective coating (doped by 20 wt% MgO NCs) were normalized to solar spectrum at AM1.5 and plotted in Figure 9. A significant overlap is observed between the fluorescence spectra and the spectral sensitivity of c-Si PV cell in the visible region of solar spectra, this phenomenon supports the power enhancement of the PV cell once attached to these LSCs coated by the UV fluorescent protective coating as depicted in Figure 1.

UV protection of LSCS by PMMA/MgO nanohybrid coatings

The change in the absorption spectra of coated and uncoated LSC samples was monitored before and after exposure natural sunlight for 35 weeks, the coated samples showed a distinct photostability since no significant change was observed in their

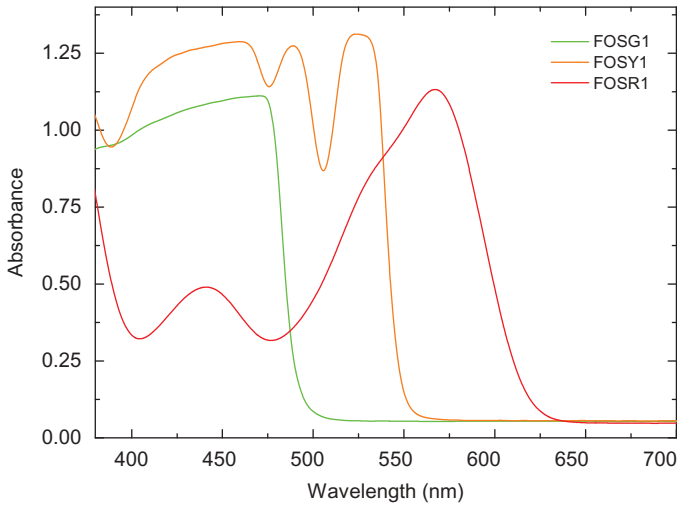

Figure 8. Visible absorption spectra for the investigated LSC plates.

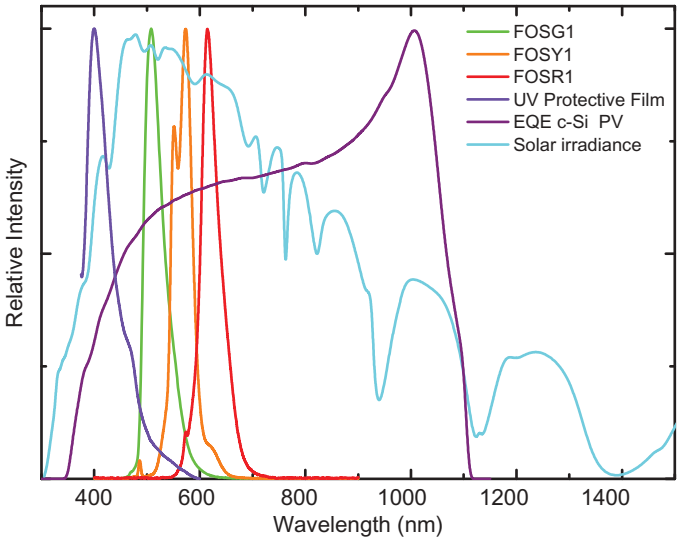

Figure 9. The external quantum efficiency (EQE) of c-Si PV cell, the fluorescence spectra of LSC plates and the optimized UV fluorescent protective film (normalized to AM1.5 solar spectrum).

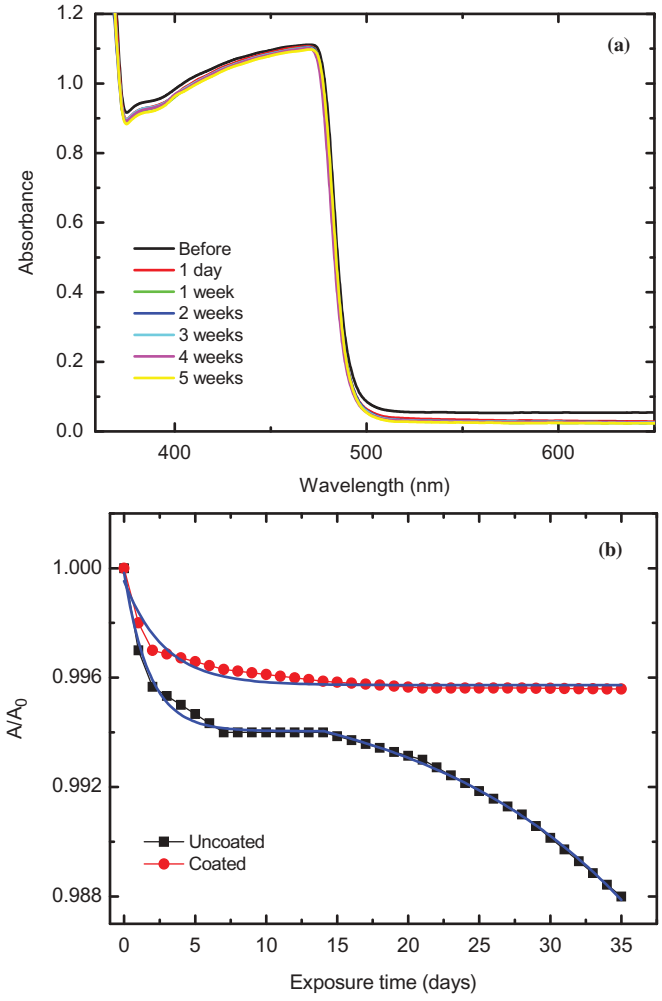

Figure 10. (a) Absorption spectra of uncoated LSC sample (FOSG1) before and after exposure to natural sunlight for 5 weeks at 32 °C and (b) The corresponding photodegradation curves before and after coating with PMMA/MgO nanocomposite film.

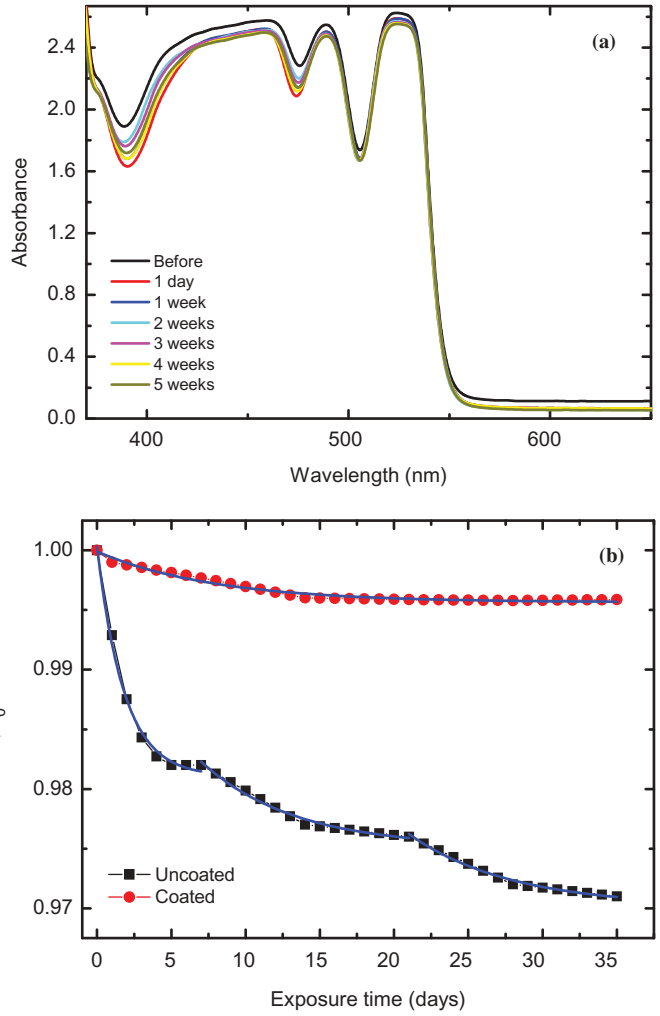

Figure 11. (a) Absorption spectra of uncoated LSC sample (FOSY1) before and after exposure to natural sunlight for 5 weeks at 32°C and (b) The corresponding photodegradation curves before and after coating with PMMA/MgO nanocomposite film.

absorption spectra, unlike other uncoated samples which have a sequentially reduced absorption as shown in Figures 10–12. The photodegradation (*P*%), which is the percentage change in the optical density after sunlight exposure for a specific time, has been calculated and plotted for coated and uncoated LSC samples as shown in Figures 10–12. It is clearly noted that all uncoated LSC samples have more than one degradation step according to the following exponential relation:

$$P\% = C_n e^{-R_n t} + A_t/A_0 \tag{9}$$

where C_n is the fitting constant, R_n is the photodegradation rate constant (n designates for the degradation step number) and A_t/A_0 is the percentage change in the absorption maxima in the visible region denoting for the remainder of the dye after the end of LSC exposure to sunlight. It is evident from Table 2 that the photodegradation mechanism for all the coated LSC samples occurs through one step with a noticeably lower degradation rate compared to uncoated LSCs.

The UV stability test had been performed as a helpful tool for determining the type of UV radiation that can be blocked by UV fluorescent protective coating. Table 3 shows the calculated

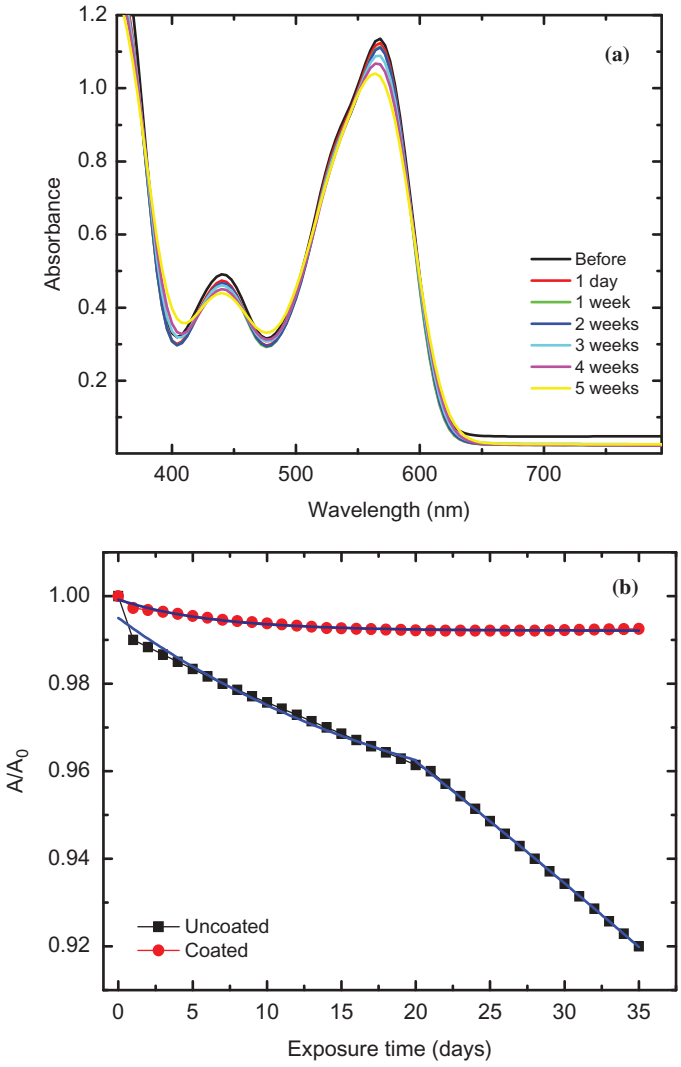

Figure 12. (a) Absorption spectra of uncoated LSC sample (FOSR1) before and after exposure to natural sunlight for 5 weeks at 32°C and (b) The corresponding photodegradation curves before and after coating with PMMA/MgO nanocomposite film.

Table 2. The photodegradation parameters of uncoated and coated LSCs exposed to natural sunlight for 5 weeks.

	Uncoated		Coated	
LSC	A_t/A_0	R_n (10^{-6}sec^{-1})	A_t/A_0	R_n (10^{-6}sec^{-1})
FOSG1	0.988	4.13 7.80	0.996	2.12
FOSY1	0.971	6.33 1.84 1.68	0.996	1.46
FOSR1	0.920	5.30 7.06	0.992	1.82

photodegradation parameters A/A_0 and R_n for coated and uncoated LSCs exposed to different types of UV radiation for 96 hr. For uncoated LSC samples, it is evident that UVA (365 nm) is the accountable part of solar spectrum that caused the photodegradation of luminescent dye molecules observed in Figures 10–12. In addition, it is clear that the uncoated LSC samples exposed to UVC (254 nm) have a more than 100% increase in the values of R_n, besides the observed drop in the values of A/A_0 which decreased to 79.8 %, 71.5 % and 82.2 % for FOSG1, FOSY1 and

Table 3. The photodegradation parameters of uncoated and coated LSCs irradiated with UV radiation for 96 hr.

	Uncoated				Coated			
	UV 254		UV 365		UV 254		UV 365	
LSC	A_t/A_0	R_n (10^{-4} sec^{-1})	A_t /A_0	R_n (10^{-6} sec^{-1})	A_t /A_0	R_n(10^{-5} sec^{-1})	A_t /A_0	R_n (10^{-6} sec^{-1})
FOSG1	0.751	3.61	0.980	4.20 7.91	0.941	4.51	0.989	2.24
FOSY1	0.692	8.12 5.10 2.34	0.969	6.51 2.06 1.82	0.968	6.12	0.990	1.51
FOSR1	0.783	6.65 7.84	0.901	5.41 8.23	0.952	9.12	0.983	1.93

FOSR1 uncoated LSC samples respectively. These results can be deeply rooted by Figure 13 which shows that the exposure to UVC caused cracks and partial detachment from the LSC samples, this can the behavior is slightly observed for LSC substrates exposed to UVB which showed a remarkably enhanced protection. This enhancement was confirmed by measuring the fluorescence spectra which showed no significant change in the fluorescence intensity for UVB exposed samples, at variance to the behavior observed for UVC exposed samples which showed a dramatic

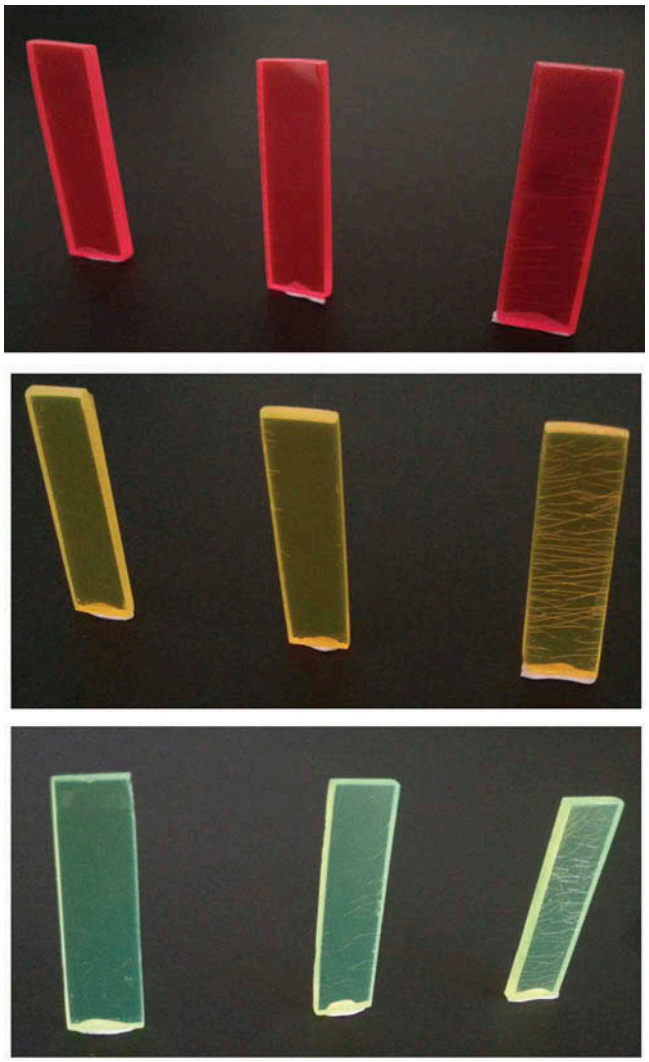

Figure 13. Surface morphology of coated LSCs before (left) and after irradiation with UVA (middle) and UVB (right).

decrease in the fluorescence intensity caused by the dye degradation as shown in Figure 14.

Figure 15 shows the *I–V* characteristics of c-Si PV cell attached coated and uncoated LSC prototypes at light intensity 100 mW/cm^2 measured along with an identical reference PV cell. The remarkable increase in the useful efficiency regimes for coated LSCs, is a direct indicator of the effective concentration ratio besides the spectral downshifting of solar spectrum in the UV region. These results are of primary importance to overcome the poor spectral response of PV modules which exhibit a poor EQE at short wavelengths (Klampaftis et al. 2009), thereby increasing the amount of photocurrent that can be generated from this part of high energy solar spectrum. The enhancement in the power conversion efficiency (η) of PV cell which is thepercentage of power converted from the absorbed light to electrical energy, had been calculated as the ratio of maximum output power (P_{out}) divided by the input light power (P_{in}) and listed in Table 4. The enhancement in the conversion power efficiency, $\Delta\eta\%$, can be calculated as follows (El-Bashir 2014a):

$$\Delta\ \eta\% = [(\eta_{LSC}\% - \eta_{PV}\%)/\eta_{PV}\%] \times 100 \qquad (10)$$

where η_{PV} % is the power conversion efficiency of reference c-Si PV cell and is the power conversion efficiency of c-Si PV cell attached to LSC prototypes. The calculated values of $\Delta\eta\%$ showed a maximum value (32.49%) for coated FOSR1 LSC, as a result of the better spectral match between the fluorescence spectrum of this plate and the EQE of c-Si PV cell as revealed by Figure 9.

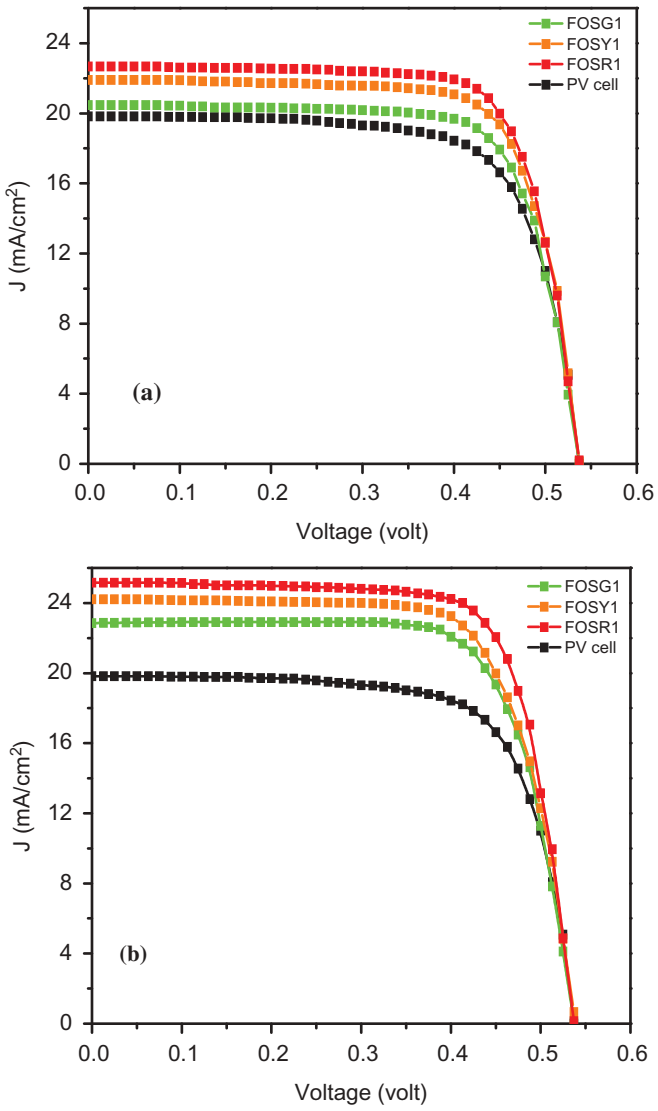

Figure 15. IV characteristics of LSCs (a) uncoated and (b) coated with PMMA/MgO nanocomposites.

Conclusions

This paper proposed solutions for two important problems that have challenged the applications of LSCs; the first problem concerned with the limited absorption and stability of commercial fluorescent PMMA plates in the UV region of solar spectrum. This had been overcome by preparing thin films of UV protective

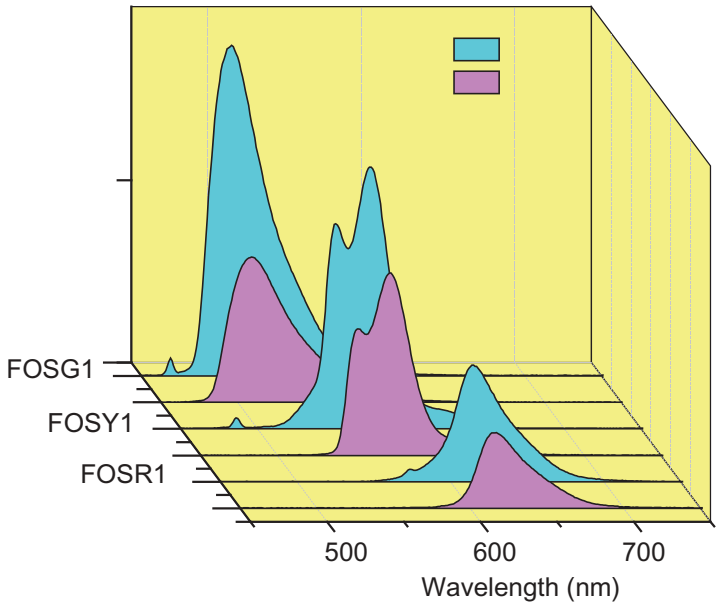

Figure 14. Fluorescence spectra of coated LSC samples after irradiation with UVB (254 nm) for 96 hr.

Table 4. The power conversion efficiency of c-Si PV cell before and after being attached to the edge of LSC prototypes.

	FOSG1		FOSY1		FOSR1	
PV cell	Uncoated	Coated	Uncoated	Coated	Uncoated	Coated
13.76	14.67	16.07	15.71	17.01	16.39	18.23

coatings based on PMMA/MgO nanohybrids in the range of 20 μm. The coatings were directly applied on commercially LSC plates that have a broad absorption in the visible region of solar spectra and luminescence covering the visible solar spectra as depicted by Figure 9 and Table 1. The second problem is the poor EQE of c-Si PV cells at short wavelengths; PMMA/MgO UV protective coatings were implemented as a luminescent down shifting layers (LDSL) that increased the power conversion efficiency of c-Si PV cell from 13.76 % to 18.23 %, achieved for coated LSC (FOSR1). In summary, the nanohybrid PMMA/MgO coatings are promising to increase the photostability and power conversion efficiency of LSCs in addition to the increase of the absorbed spectral range of sunlight.

Acknowledgments

This research project was supported by a grant from the Deanship of Scientific Research, Princess Nora Bint Abdul Rahman University (34-K-47). The authors are grateful to Prof.Dr. Hab. GrzegorzKarczewski, the head of the group of physics of quantum structures, Institute of Physics, Polish academy of Science, Warsaw, Poland; for supporting the quantum efficiency measurements of c-Si PV solar cell.

References

Batchelder, J. S., A. H. Zewail, and T. Cole. 1979. Luminescent solar concentrators. 1: Theory of operation and techniques for performance evaluation. *Applied Optics* 18:3090–110.doi:10.1364/AO.18.003090.

Callister, W. D. 1997. *Materials Science and Engineering— An Introduction*. New York, NY: John-Wiley and Sons.

Carlotti, M., G. Ruggeri, F. Bellina, and A. Pucci. 2016. Enhancing optical efficiency of thin-film luminescent solar concentrators by combining energy transfer and stacked design. *Journal of Luminescence* 171:215–20. doi:10.1016/j.jlumin.2015.11.010.

Crosby, G. A., and J. N. Demas. 1971. Measurement of photoluminescence quantum yields. Review. *The Journal of Physical Chemistry* 75:991–1024. doi:10.1021/j100678a001.

Cullity, B. D. 1956. *Elements of X-ray Diffraction*. Boston, MA: Addison-Wesley.

Dadvar, S., H. Tavanai, and M. Morshed. 2011. UV-protection properties of electro spun polyacrylonitrile nanofibrous mats embedded with MgO and Al_2O_3 nanoparticles. *Journal of Nanoparticle Research* 13:5163–69. doi:10.1007/s11051-011-0499-4.

De Boer, D. K., D. J. Broer, M. G. Debije, W. Keur, A. Meijerink, C. R. Ronda, and P. P. Verbunt. 2012. Progress in phosphors and filters for luminescent solar concentrators. *Optics Express* 20:A395–A405. doi:10.1364/OE.20.00A395.

Debije, M. G., and P. P. Verbunt. 2012. Thirty years of luminescent solar concentrator research: Solar energy for the built environment. *Advanced Energy Materials* 2:12–35.doi:10.1002/aenm.201100554.

Dienel, T., C. Bauer, I. Dolamic, and D. Brühwiler. 2010. Spectral-based analysis of thin film luminescent solar concentrators. *Solar Energy* 84:1366–69. doi:10.1016/j.solener.2010.04.015.

Du Pasquier, A., S. Miller, and M. Chhowalla. 2006. On the use of Ga–In eutectic and halogen light source for testing P3HT–PCBM organic solar cells. *Solar Energy Materials and Solar Cells* 90:1828–39. doi:10.1016/j.solmat.2005.11.003.

Edwards, M., S. Bowden, U. Das, and M. Burrows. 2008. Effect of texturing and surface preparation on lifetime and cell performance in heterojunction silicon solar cells. *Solar Energy Materials and Solar Cells* 92:1373–77. doi:10.1016/j.solmat.2008.05.011.

El-Bashir, S. M. 2012. Photophysical properties of fluorescent PMMA/SiO_2nanohybrids for solar energy applications. *Journal of Luminescence* 132:1786–91. doi:10.1016/j.jlumin.2012.02.010.

El-Bashir, S. M., O. A. AlHarbi, and M. S. AlSalhi. 2013a. Thin-Film LSCs Based on PMMA Nanohybrid Coatings: Device Optimization and Outdoor Performance. *International Journal of Photoenergy* 2013:1–10. doi:10.1155/2013/235875.

El-Bashir, S. M., O. A. AlHarbi, and M. S. AlSalhi. 2014a. Optimal design for extending the lifetime of thin film luminescent solar concentrators. *Optik-International Journal for Light and Electron Optics* 125:5268–72. doi:10.1016/j.ijleo.2014.06.046.

El-Bashir, S. M., F. M. Barakat, and M. S. AlSalhi. 2013b. Metal-enhanced fluorescence of mixed coumarin dyes by silver and gold nanoparticles: Towards plasmonic thin-film luminescent solar concentrator. *Journal of Luminescence* 143:43–49. doi:10.1016/j.jlumin.2013.04.029.

El-Bashir, S. M., F. M. Barakat, and M. S. AlSalhi. 2014b. Double layered plasmonic thin-film luminescent solar concentrators based on polycarbonate supports. *Renewable Energy* 63:642–49. doi:10.1016/j.renene.2013.10.014.

Goldschmidt, J. C., M. Peters, A. Bösch, H. Helmers, F. Dimroth, S. W. Glunz, and G. Willeke. 2009. Increasing the efficiency of fluorescent concentrator systems. *Solar Energy Materials and Solar Cells* 93:176–82. doi:10.1016/j.solmat.2008.09.048.

Griffini, G., M. Levi, and S. Turri. 2013. Novel crosslinked host matrices based on fluorinated polymers for long-term durability in thin-film luminescent solar concentrators. *Solar Energy Materials and Solar Cells* 118:36–42. doi:10.1016/j.solmat.2013.05.041.

Griffini, G., M. Levi, and S. Turri. 2014. Novel high-durability luminescent solar concentrators based on fluoropolymer coatings. *Progress in Organic Coatings* 77:528–36. doi:10.1016/j.porgcoat.2013.11.016.

Hammam, M., M. K. El-Mansy, S. M. El-Bashir, and M. G. El-Shaarawy. 2007. Performance evaluation of thin-film solar concentrators for greenhouse applications. *Desalination* 209:244–50. doi:10.1016/j.desal.2007.04.034.

International Centre for Diffraction Data. 2002. JCDPS, PCPDFWIN, V.2.3, (pp. 89–4248).

Kittel, G. 1976. *Introduction to Solid State Physics*, 5th ed. New York, NY: John Wiley and Sons.

Klampaftis, E., D. Ross, K. R. McIntosh, and B. S. Richards. 2009. Enhancing the performance of solar cells via luminescent down-shifting of the incident spectrum: A review. *Solar Energy Materials and Solar Cells* 93:1182–94. doi:10.1016/j.solmat.2009.02.020.

Murali, K. R., A. Kalaivanan, S. Perumal, and P. N. Neelakanda. 2010. Sol–gel dip coated CdO: Al films. *Journal Alloys & Compounds* 503:350–53. doi:10.1016/j.jallcom.2009.11.187.

Roncali, J., and F. Garnier. 1984. Photon-transport properties of luminescent solar concentrators: Analysis and optimization. *Applied Optics* 23:2809–17.doi:10.1364/AO.23.002809.

Rowan, B. C., L. R. Wilson, and B. S. Richards. 2008. Advanced material concepts for luminescent solar concentrators. *IEEE Journal of Selected Topics in Quantum Electronics*14:1312–22. doi:10.1109/JSTQE.2008.920282.

Stankic, S., M. Müller, O. Diwald, M. Sterrer, E. Knözinger, and J. Bernardi. 2007. Size-Dependent Optical Properties of MgONanocubes. *Angewandte Chemie International Edition* 44:4917–20. doi:10.1002/anie.200500663.

Wiegman, J. W. E., and E. Van Der Kolk. 2012. Building integrated thin film luminescent solar concentrators: Detailed efficiency characterization and light transport modelling. *Solar Energy Materials and Solar Cells* 103:41–47. doi:10.1016/j.solmat.2012.04.016.

Yahia, I. S., F. Yakuphanoglu, and O. A. Azim. 2011. Unusual photocapacitance properties of a mono-crystalline silicon solar cell for optoelectronic applications. *Solar Energy Materials and Solar Cells* 95:2598–605. doi:10.1016/j.solmat.2011.05.001.

Zhang, Y., W. Xiao, L. Yongxin, S. Shuyan, and L. Dapeng. 2012. Highly transparent bulk PMMA/ZnO nanocomposites with bright visible luminescence and efficient UV-shielding capability. *Journal of Materials Chemistry* 22:11971–77. doi:10.1039/c2jm30672g.